Supplementary Information (SI) for Journal of Materials Chemistry A.

This journal is © The Royal Society of Chemistry 2025

Supporting information

Room-temperature self-healing and mechanically robust siloxane elastomer via synergistic complexation and cation-π interactions for high-performance electromagnetic interference shielding

Suting Chen[‡a], Ziyi Liu[‡a], Tian Qiu[a], Ting Zhang[a], Chaoqun Ma[b], Dongjin Xie[a], Tengning Ma[a], Li Yang[a], Guanjun Chang*[a] and Ying Huang*[a]

[a]State Key Laboratory of Environment-friendly Energy Materials & School of Materials and Chemistry, Southwest University of Science and Technology, Mianyang, 621010, China

[b]School of Materials Science and Engineering, University of Science and Technology Beijing, Beijing, 100083, China

*Corresponding authors.

‡These authors contributed equally.

E-mail: gjchang@mail.ustc.edu.cn; huangy@swust.edu.cn

Preparation of 2-phenyl-1H-indol-3-amine (IN)

A solution of 2-phenylindole (2-IN) (5 g, 25.87 mmol) in glacial acetic acid (50 mL) was cooled to 18°C in an ice bath. An aqueous solution of sodium nitrite (1.60 g, 23.19 mmol in 3 mL deionized water) was added dropwise. The reaction mixture was stirred at room temperature for 30 min, then diluted with ice water (250 mL). The resulting precipitate was collected by filtration, washed with water and recrystallized from methanol, and dried to obtain 3-nitroso-2-phenyl-1H-indole (NO-IN). NO-IN (25 g, 0.129 mol) was dissolved in ethanol (450 mL), followed by addition of 2 M NaOH solution (300 mL). Sodium dithionite (38 g) was added, and the reaction mixture was heated to reflux at 80 °C for 5 h. After cooling, the precipitate was collected by filtration, washed with water, recrystallized from methanol, and dried to obtain 2-phenyl-1H-indol-3-amine (IN).

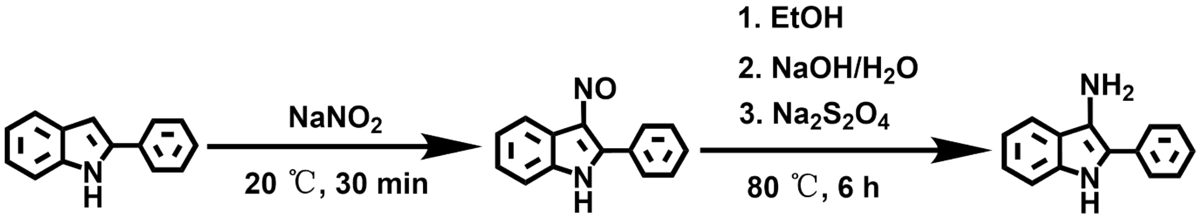

Figure S1. Synthesis route of IN.

Characterization

Fourier-transform infrared (FTIR) spectroscopy was performed in transmission mode using a Nicolet 6700 spectrometer (Thermo-Fisher Scientific, USA) over the range of 4000-400 cm^{-1}. Nuclear magnetic resonance (NMR) spectroscopy was conducted using a Bruker Avance 600 spectrometer with DMSO as the solvent. Ultraviolet and visible (UV-vis) absorption spectra were obtained on a Shimadzu UV-2600 spectrophotometer. The fluorescence emission spectra were performed by using an RF-6000 spectrophotometer under an excitation wavelength of

365 nm, with excitation and emission slit widths of 3.0 nm and 5.0 nm, respectively. X-ray photoelectron spectroscopy (XPS) was employed to investigate the chemical composition of the samples using a Thermo Scientific K-ALPHA spectrometer equipped with an monochromatized Al target (E = 1486.68 eV). X-ray diffraction (XRD) patterns were recorded using an X-ray diffractometer (X'Pert Pro, Panalytical, Netherlands) over a 2θ range of 5-80°. Glass transition temperatures were measured using a differential scanning calorimeter (DSC) instrument (DSC Q2000, TA, USA) at a heating rate of 10 ℃/min from -50 ℃ to 50 ℃ under a nitrogen atmosphere. Thermogravimetric analysis (TGA) was conducted on a TGA Q500 thermoanalyzer (TA, USA) at a heating rate of 20 ℃ min^{-1} under a nitrogen atmosphere. Rheological measurements were performed using a rheometer (Anton Paar, MCR 102e, Austria) equipped with parallel plates (25 mm diameter). The frequency sweep tests were carried out at a rotational strain amplitude of 0.1%, varying the frequency from 0.1 rad s^{-1} to 100 rad s^{-1} at 0°C and 25°C. Morphological analysis was conducted using scanning electron microscopy (SEM, Zeiss Ultra 55, Germany). Mechanical properties were evaluated using a universal tensile testing machine (E44.104, MTS). Electrical conductivity was measured by the standard four-probe method on a physical property measurement system (RTS-9, Guangzhou, China) at room temperature. The EMI shielding performance were obtained using a vector network analyzer (3656D, China) via the waveguide method in the 8.2-12.4 GHz region. The coefficients of reflectance (R), absorption (A) and transmittance (T) as well as EMI shielding effectiveness were calculated from the scattering parameters (S_{11} and S_{21}) by the following equations (1)-(6):

$$R = |S_{11}|^2 \tag{1}$$

$$T = \left|S_{21}\right|^2 \tag{2}$$

$$A = 1 - R - T \tag{3}$$

$$SE_T\left(dB\right) = -10\log T \tag{4}$$

$$SE_R\left(dB\right) = -10\log\left(1 - R\right) \tag{5}$$

$$SE_A\left(dB\right) = -10\log\left(\frac{T}{1 - R}\right) \tag{6}$$

Where SE_T is the total EMI shielding effectiveness, SE_A is the absorption effectiveness, and SE_R is the reflection effectiveness.

Theoretical calculations

Electrostatic potential of indole derivative, and HOMO-LUMO orbitals of indole derivative and its complex was performed using the DMol^3 module in Materials Studio. The exchange-correlation functional was described by the generalized gradient approximation (GGA) with the BLYP or PBE functional.

Molecular dynamics (MD) simulation was performed using the Forcite module with a universal force field of Materials Studio. A parent INPDMS chain with 10 repeating units was built, with 100% repeating units including indole derivative group. Fe^{3+} ions were randomly distributed on the polymer chain with concentrations matching experimental data. Although size of the parent INPDMS chain was not sufficiently long to represent conformations of a real polymer chain, a previous study has reported a good agreement between experiments and simulations when simulated polycarbonate chains were short (merely 10-15 repeat units on average).[1] Moreover, a periodic boundary condition was imposed and an initial density of 0.9

g/cm^3 was used to simulate the polymer conformation in bulk under an equilibrium state. The initial structure was optimized by molecular mechanics technique using the conjugate gradient method. Because this optimized structure might still be in a local energy minimum state, the polymer in simulation box was relaxed through NVT for 100 ps at 800 K with time steps of 1.0 fs. The simulation of high-temperature relaxation was closely followed a protocol suggested previously.[2] After 100 ps of simulated relaxation at 800 K, the system temperature was decreased to 273 K. In order to obtain a suitable structure for further analysis, twenty different initial structures for each system were built and relaxed according to the procedure mentioned previously. The one with the lowest system energy was selected as the MD result for further analysis.

The radial distribution function, $g_{AB}(r)$, was introduced to describe how density of designated particles varies as a function of distance from a reference particle. Usually, $g_{AB}(r)$ is determined by measuring the ensemble averaged distance between all particle pairs, as follows,

$$g_{AB}(r) = \frac{\langle n_{AB}(r) \rangle}{4\pi r^2 \Delta\rho_{AB}}$$

where, $n_{AB}(r)$ is the distance of each pair between A (Fe^{3+}) and B (indole derivative) in the simulation box. <...> represents an ensemble average. $\Delta\rho_{AB}$ is the rate of change in the average number density of Fe^{3+} over distance from an indole ring. The plot of $g_{AB}(r)$ gives the local density of B around A at a distance r. $g_{AB}(r) = 1$ indicate the particles are completely uncorrelated. A positive peak of $g_{AB}(r)$ reflects a definite correlation between atoms at r.

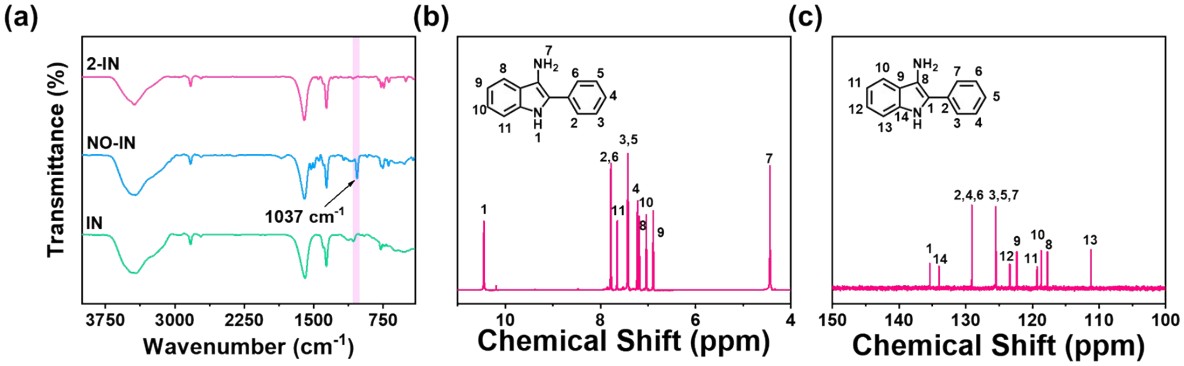

Figure S2. (a) FTIR spectra of 2-IN, NO-IN and IN. (b) ^{1}H NMR spectrum of IN. (c) ^{13}C NMR spectrum of IN.

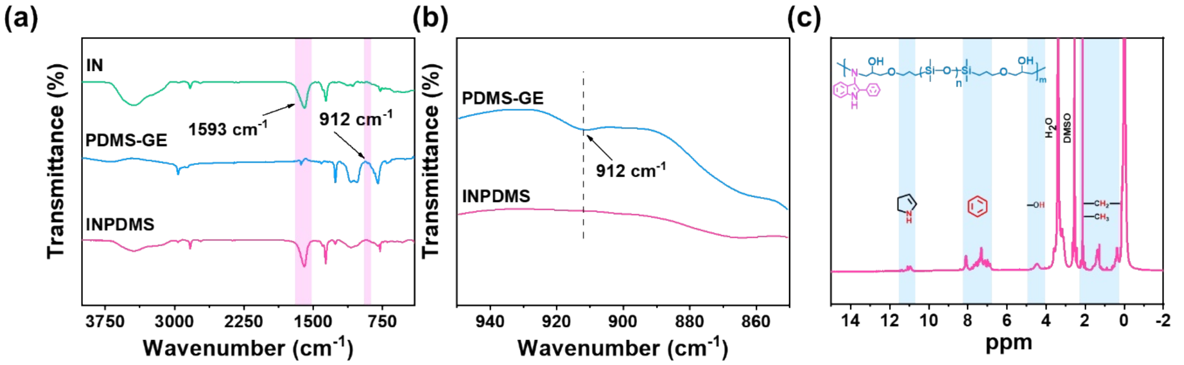

Figure S3. (a) FTIR spectra of IN, PDMS-GE and INPDMS. (b) Enlarged FTIR spectra of PDMS-GE and INPDMS. (c) ^{1}H NMR spectrum of INPDMS.

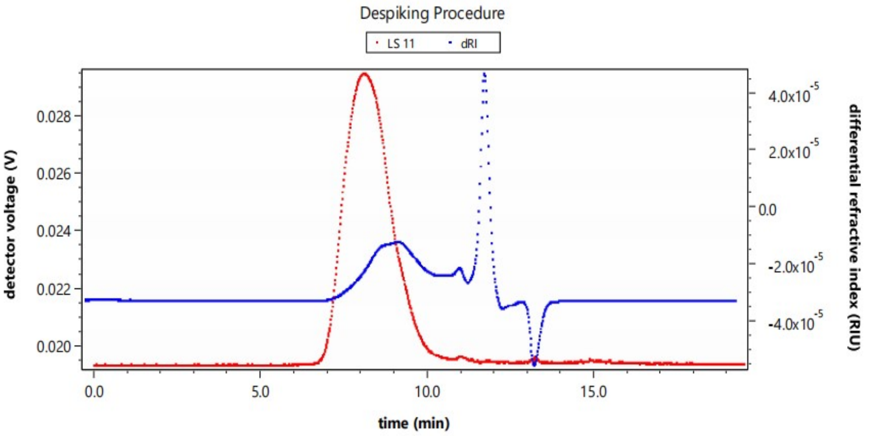

Figure S4. GPC curve of INPDMS.

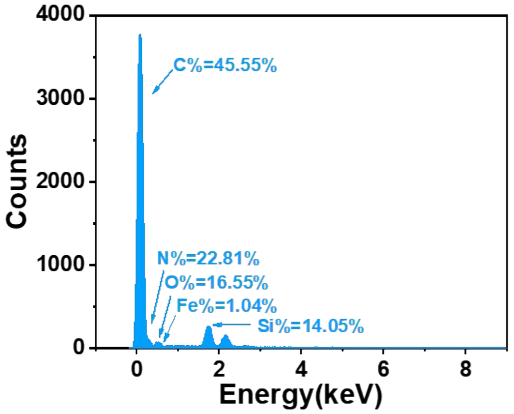

Figure S5. EDS spectrum of INPDMS-Fe-x.

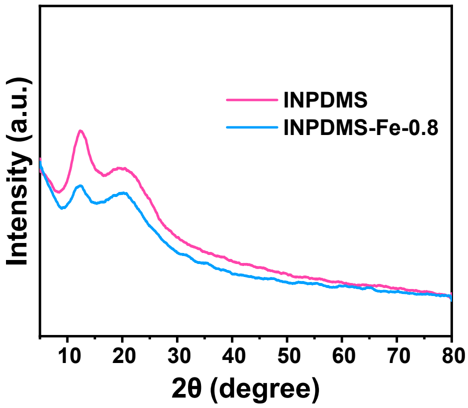

Figure S6. XRD patterns of INPDMS and INPDMS-Fe-0.8.

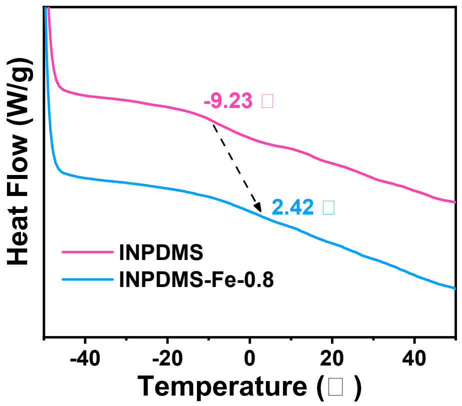

Figure S7. DSC curves of INPDMS and INPDMS-Fe-0.8.

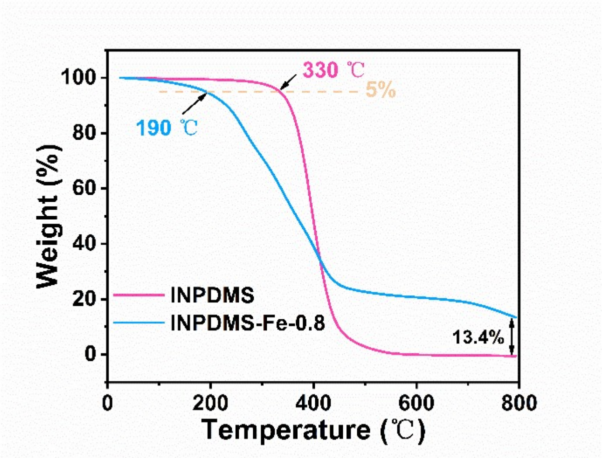

Figure S8. TGA curves of INPDMS and INPDMS-Fe-0.8.

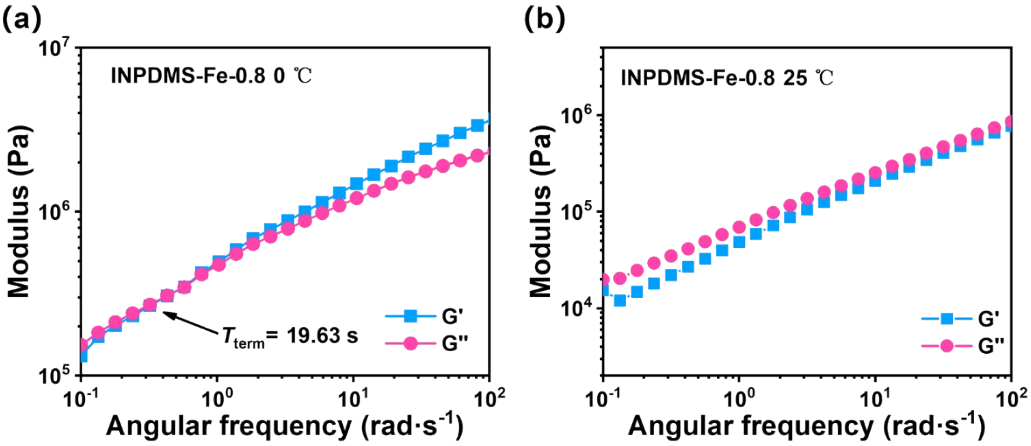

Figure S9. Rheological master curves showing the frequency dependency of the storage modulus (G′) and loss modulus (G″) for INPDMS-Fe-0.8 at a reference temperature of (a) 0°C and (b) 25°C.

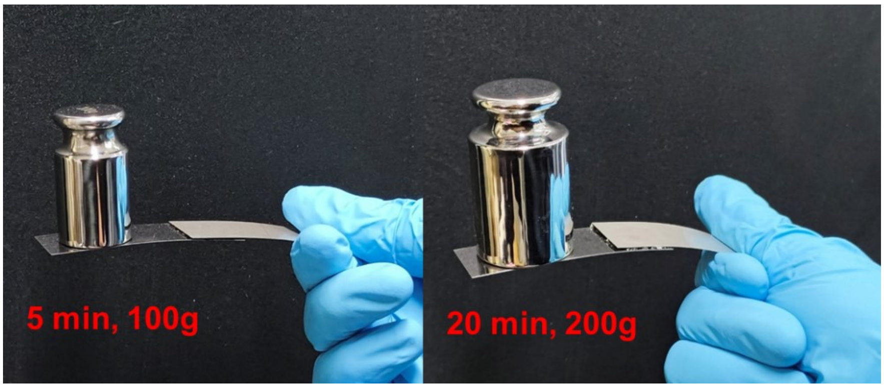

Figure S10. Digital photos of load-bearing demonstration.

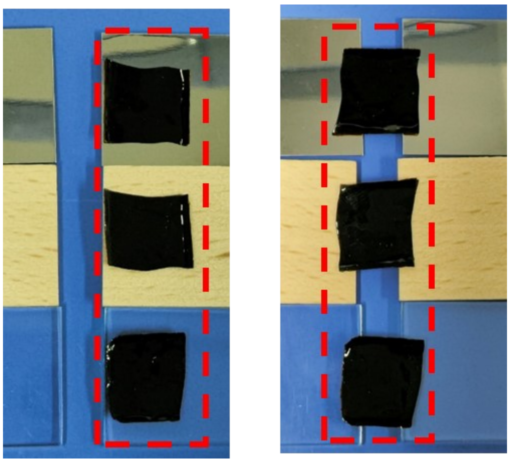

Figure S11. Reusability and peel-off behavior.

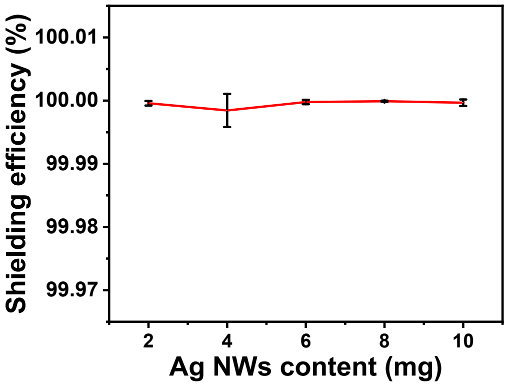

Figure S12. Shielding efficiency of Ag NWs/INPDMS-Fe-0.8 composite films.

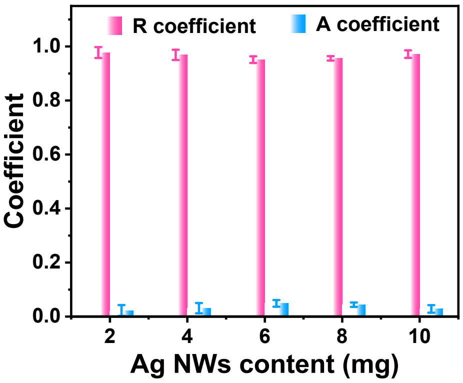

Figure S13. R-A plots of Ag NWs/INPDMS-Fe-0.8 composite films.

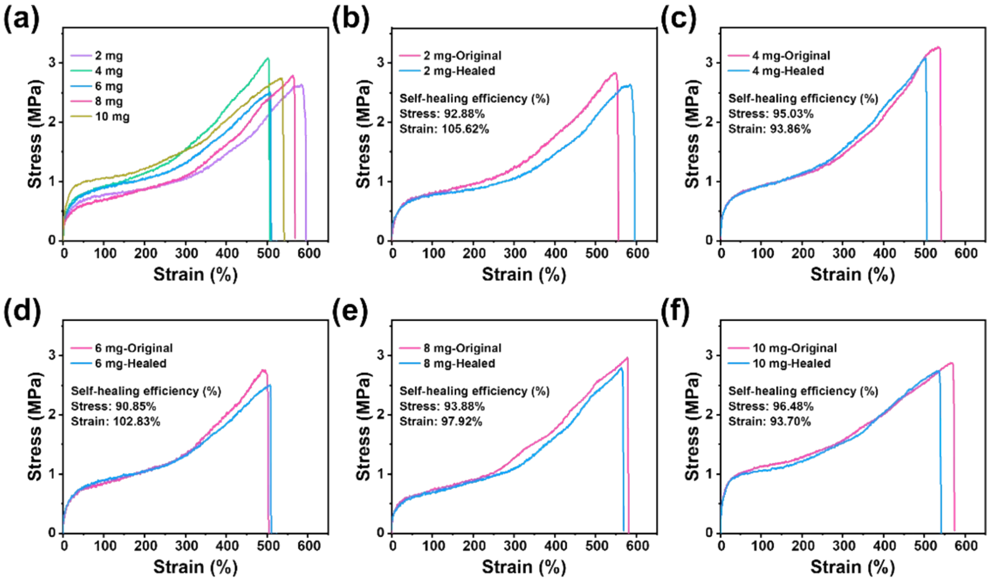

Figure S14. (a) Stress-strain curves of composite films with different Ag NWs loading after self-healing. Stress-strain curves of composite films before and after self-healing with different Ag NWs loading: (b) 2 mg, (c) 4 mg, (d) 6 mg, (e) 8 mg, and (f) 10 mg.

Table S1. Formulation of INPDMS-Fe-x

Samples	INPDMS (g)	$FeCl_3$ (mmol)
INPDMS-Fe-0.2	1	0.2
INPDMS-Fe-0.4	1	0.4
INPDMS-Fe-0.6	1	0.6
INPDMS-Fe-0.8	1	0.8
INPDMS-Fe-1.0	1	1.0

Reference

[1] C. F. Fan, T. Cagin, Z. M. Chen, K. A. Smith, *Macromolecules*, 1994, **27**, 2383.

[2] K. J. Lee, W. L. Mattice, R. G. Snyder, *J. Chem. Phys.*, 1992, **96**, 9138.